



A Reappraisal of Seismicity Recorded During the 1996 Gjalp Eruption, Iceland, in Light of the 2014–2015 Bárðarbunga–Holuhraun Lateral Dike Intrusion

K. I. KONSTANTINO¹ , I. WAHYU UTAMI¹, D. GIANNOPOULOS^{2,3} and E. SOKOS⁴

Abstract—This study performs a reanalysis of the seismicity recorded during the 1996 Gjalp eruption that occurred at NW Vatnajökull, Iceland. The seismicity was recorded by the temporary HOTSPOT network consisting of 30 three-component broadband stations. In total 301 events were identified between 29 September and 12 October and their phases were manually picked. A velocity model was estimated from P-phase travel times by using VELEST. Events were first located using the algorithm NON-LINLOC in order to obtain absolute locations. Precise relative locations were obtained with HYPODD by utilizing catalog and cross-correlation differential travel times. Results show that events clustered first along the SW rim of the Bárðarbunga caldera and later along the Gjalp fissure, with most hypocentral depths located between 3 and 8 km. Waveforms of the 10 largest events that followed the Bárðarbunga earthquake were inverted in order to obtain moment tensors. For all events we found that the deviatoric moment tensor fits the data better than pure double-couple or full moment tensor solutions. Events along the Bárðarbunga caldera exhibited reverse focal mechanisms, while those at the Gjalp fissure exhibited mostly strike-slip faulting. Seismic velocity variations calculated using ambient noise interferometry, point to the possibility that a small subglacial eruption occurred at Bárðarbunga before the main earthquake. This removed melt from the magma chamber causing its roof to collapse, and also resulted in the lateral migration of magma towards the Gjalp fissure. The 2014–2015 Bárðarbunga–Holuhraun eruption shares common characteristics with the 1996 Gjalp eruption, although the size of the latter was much smaller.

Keywords: Gjalp, Bárðarbunga, Vatnajökull, eruption, seismicity, Iceland.

1. Introduction

Iceland was created as a result of the interaction of the Mid-Atlantic Ridge and a mantle plume that is currently located beneath the central part of the island, extending down to a depth of 400 km within the mantle (Tryggvason et al. 1983; Wolfe et al. 1997; Shen et al. 1998). This interaction is responsible for much of the observed volcanic activity in Iceland, as manifested by the existence of more than 30 active volcanoes (Thordarson and Larsen 2007). Volcanism is focused on three axial rift zones that correspond to the main sites of active spreading (Fig. 1). Each of these zones encompasses a number of volcanic systems and each of these systems consist of a central volcano as well as a transecting fissure swarm. Most of the fissure swarms have widths of 10–20 km, lengths of 50–100 km and they are usually associated with one or more central volcanoes. Eruptive activity in these volcanoes is maintained by a long-lived plumbing system and their overall architecture is determined by the type of magma erupted and the environmental setting (either subglacial or subaerial) where such an eruption occurs (Thordarson and Larson 2007).

Vatnajökull glacier, located in the central part of Iceland, occupies an area of about 8100 km² and the average thickness of its ice is in the order of 380 m (Björnsson 1988) (cf. Fig. 1). Underneath the glacier lie several volcanic systems and two of them, namely Bárðarbunga and Grimsvötn, have been by far the most active during historical times (Björnsson and Einarsson 1990; Björnsson and Gudmundsson 1993). Grimsvötn is Iceland's most active volcano with 75 known eruptions in the last 1100 years (Larsen 2002) while it also exhibits high geothermal activity. Eruptions associated with Grimsvötn are often

Electronic supplementary material The online version of this article (<https://doi.org/10.1007/s00024-019-02387-x>) contains supplementary material, which is available to authorized users.

¹ Department of Earth Sciences, National Central University, Jhongli, Taoyuan City 320, Taiwan. E-mail: kkonst@ncu.edu.tw

² Seismotech S. A., 15123 Athens, Greece.

³ Laboratory of Geophysics & Seismology, Department of Natural Resources & Environment, Hellenic Mediterranean University, Chania, Greece.

⁴ Seismological Laboratory, University of Patras, 26504 Rio, Greece.

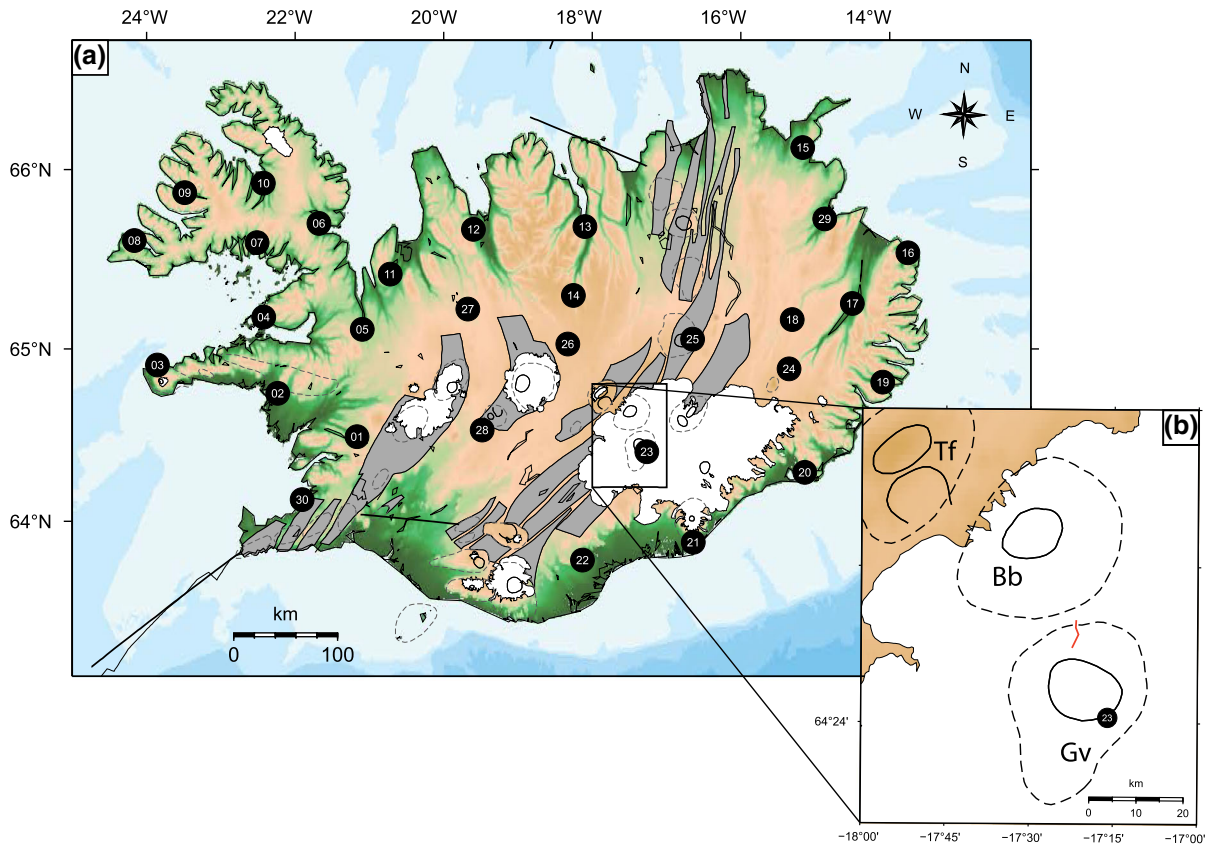


Figure 1

a Map of Iceland depicting the main rift zones, their central volcanoes and the location of the HOTSPOT seismic stations. Gray shaded areas represent rift zones, solid lines represent caldera outlines while dashed lines indicate the extent of central volcanoes. Thick solid lines represent large fracture zones. White areas are permanent glaciers, the largest of them being Vatnajökull in the center. HOTSPOT stations are shown as black circles with a number which corresponds to the code of each station. The rectangle provides a border for the area of NW Vatnajökull where Bárðarbunga and Grimsvötn volcanoes are situated. The inset **b** at the lower right corner gives an enlarged map of this area and the red line shows the extent of the Gjalp fissure on the ice after Gudmundsson et al. (1997) (Tf: Tungnafellsjökull, Bb: Bárðarbunga, Gv: Grimsvötn)

associated with jökulhlaups, a type of glacial outburst flood that occurs when high heat transfer rates produce large volumes of meltwater. In contrast, Bárðarbunga has erupted 26 times in the last 1100 years (Gudmundsson and Högnadóttir 2007) with the most recent eruption occurring in 2014–2015. This eruption, also known as Bárðarbunga–Holuhraun eruption, started with the lateral injection of melt from the Bárðarbunga magma chamber first towards the SE and later along a NE–SW oriented dike, leading to the collapse of the magma chamber roof (Gudmundsson et al. 2014; Riel et al. 2015; Sigmundsson et al. 2015; Gudmundsson

et al. 2016; Ágústsdóttir et al. 2016; Ruch et al. 2016). Within a few days the dike propagated outside the Vatnajökull glacier and reached the surface in the area of Holuhraun. Bárðarbunga has also been the site of unusual seismic activity that started occurring around the volcano since 1973 initially in the form of small magnitude ($M_L \sim 3.9$) earthquakes (Bjarnason 2014). The first moderate event (M_w 5.4) occurred in 1977 and it was followed by a series of moderate to large events that exhibited highly non-double-couple focal mechanisms and vertical T-axes (Nettles and Ekström 1998).

On 30 September 1996 an eruption occurred in the area between Bárðarbunga and Grimsvötn, forming a 7 km long fissure on the ice which was given the name “Gjalp” (Gudmundsson et al. 1997). The Gjalp eruption was preceded one and a half days before by an earthquake with moment magnitude 5.6, located at Bárðarbunga, followed by numerous smaller events and volcanic tremor until 12 October (Konstantinou et al. 2000). The eruption produced a large volume of meltwater that drained underneath the glacier towards the south coast, generating a catastrophic jökulhlaup in early November. Earlier studies of the Gjalp eruption had focused on the Bárðarbunga earthquake source properties (Nettles and Ekström 1998; Zobin 1999; Konstantinou et al. 2003; Tkalčić et al. 2009; Fichtner and Tkalčić 2010), the source characteristics of volcanic tremor (Konstantinou 2002), or presented a preliminary analysis of the seismicity (Einarsson et al. 1997; Konstantinou et al. 2000). However, modern seismological techniques in the areas of earthquake location and in the detection of eruption precursors have since been developed that could be applied to data from past eruptions. Having this in mind, we reanalyze the seismicity recorded during the Gjalp eruption in order to obtain a better understanding of its physical mechanism. First, we give a brief description of the available dataset and how we derived an optimum velocity model that can be used for earthquake location. We then obtain relative locations by using catalog as well as cross-correlation differential travel times and derive moment tensors of events by inverting three-component waveforms. Ambient noise interferometry is used in order to calculate seismic velocity variations in an effort to detect changes prior to the onset of the eruption. Finally, we discuss our results and compare them to the seismicity observed during the 2014–2015 Bárðarbunga–Holuhraun eruption for the purpose of extracting conclusions about the physical mechanism of eruptions beneath the Vatnajökull glacier.

2. Data

The data utilized in this study was recorded by the HOTSPOT temporary seismic network that was

installed in the summer of 1996 in Iceland as a joint project of the Icelandic Meteorological Office, Princeton and Durham Universities and the United States Geological Survey (cf. Fig. 1). The primary aim of HOTSPOT was to collect data that would be used for the tomographic imaging of the mantle plume beneath Iceland (Pritchard 2000), therefore the network had good azimuthal coverage in the area around the Vatnajökull glacier. In total 30 stations were installed and each of them was equipped with a three-component sensor (either CMG-3T, CMG-40T, or CMG-3ESP) recording continuously at an interval of 20 samples per second. During the main phase of the Gjalp eruption (29 September until 12 October) all of the HOTSPOT stations were operational except from HOT11, HOT20, HOT26 and HOT30. Initially, waveforms were visually inspected in order to identify earthquakes that were recorded by at least 5 stations distributed around the site of the Gjalp eruption. A necessary condition for including an earthquake in our dataset was to observe clear P-/S-phases at station HOT23. This station was the closest station to the eruption site and recorded continuously without interruption until 12 October. This procedure yielded a total of 301 earthquakes whose P- and S-phases were manually picked and initial locations were obtained by using the velocity model of Bjarnasson et al. (1993) that was derived from the results of the ICEMELT experiment.

3. Estimation of Optimum Velocity Model

The quality of earthquake locations depends heavily on the proper choice of velocity model, therefore we used the package VELEST (Kissling 1995) in order to obtain a minimum 1D velocity model with station delays. A minimum 1D model can be defined as the velocity model that produces the smallest possible location error for a set of events (Kissling et al. 1994). VELEST attempts to solve both for the hypocenters and the most appropriate velocity model for a given set of earthquakes by inverting their corresponding travel times. The minimum 1D model found after any single VELEST run depends on the initial model from which the search begins. Therefore to avoid being trapped at a local

minimum a series of runs using different initial models is needed. Data used for the computation of the minimum 1D model should be of high quality and sample the target region evenly. In this study, the selection process was based on three criteria: (a) an azimuth gap of less than 120° , (b) at least 6 P-phase observations, and (c) an RMS residual of less than 0.5 s. A total of 98 events from the original dataset conformed to the aforementioned criteria and their travel times were subsequently used in the inversion. A family of 180 initial models was constructed by using the IASPEI91 model as a base and randomly perturbing the values of the P-wave velocities each time. The thickness of each layer was set to 2 km above the depth of 20 km, while below this we added two layers with 5 km thickness. We opted for inverting only the P-wave travel times, since S-phases were not only fewer in number, but were also associated with higher picking uncertainties.

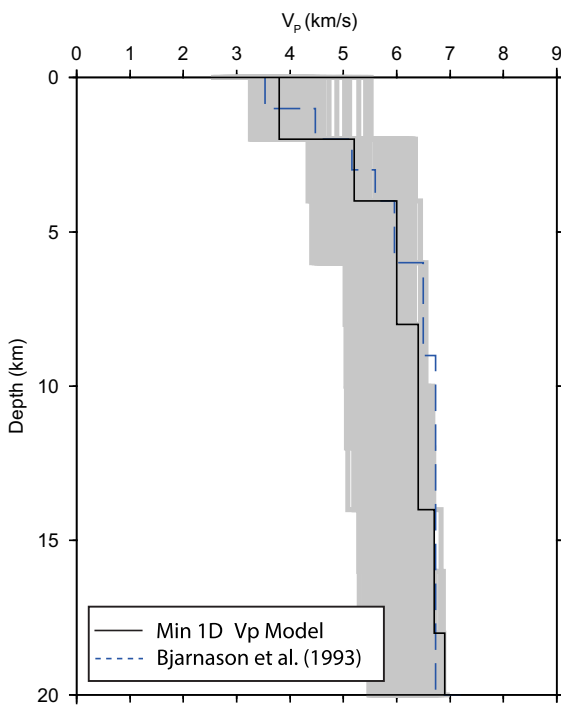


Figure 2

Diagram showing P-wave velocity as a function of depth for initial and the final velocity model inverted using VELEST. The gray lines represent 180 initial models whose velocities were randomly perturbed (see text for details). The black line indicates the final model with the lowest RMS residual that is compared to the 1D velocity model of Bjarnason et al. (1993)

Figure 2 shows the 180 initial models along with the final model that exhibited the smallest RMS residual. The velocity model is well-constrained from about 5 km down to 15 km, as a result of almost vertical rays sampling the former depth, and too few rays propagating beyond the latter depth. We carried out tests for the purpose of assessing the quality and stability of this minimum 1D velocity model. First, we shifted the initial hypocentral locations randomly in each direction by 5 km before using them as input to VELEST. The reasoning behind such a test is that if the proposed model is indeed a robust minimum in the solution space, then there should be no significant changes in the locations after the inversion. We find that all events are relocated less than 1 km from their original positions. The second test has to do with the relationship of station delays with the surface geology, in the sense that the positive/negative values of station delays should reflect the near-surface velocity structure. Station delays are calculated relative to a reference station whose installation site is well-known in terms of near-surface geology. Station HOT23 installed on a lava outcrop, was chosen as the reference station since it is located in the center of the network and has recorded the largest number of P-phases. We observe positive delays at stations HOT12, HOT13, HOT21, and HOT29 that are installed on hyaloclastite and/or sediment deposits (Fig. 3). On the other hand, all other stations that lie on basic and acidic lavas exhibit a variable amount of negative delay. Table S1 in the supplementary material gives a list of calculated delays per HOT-SPOT station.

4. Earthquake Relocation

For obtaining absolute locations of the Gjálp eruption events we employed the package NON-LINLOC which solves the earthquake location problem by using a nonlinear probabilistic algorithm (for details see Lomax et al. 2000, 2009). The Oct-Tree sampling algorithm (Lomax and Curtis 2001) was utilized as the nonlinear search method; it applies a recursive subdivision and sampling of cells in 3D space. The minimum 1D V_p model derived previously was used in order to calculate theoretical travel

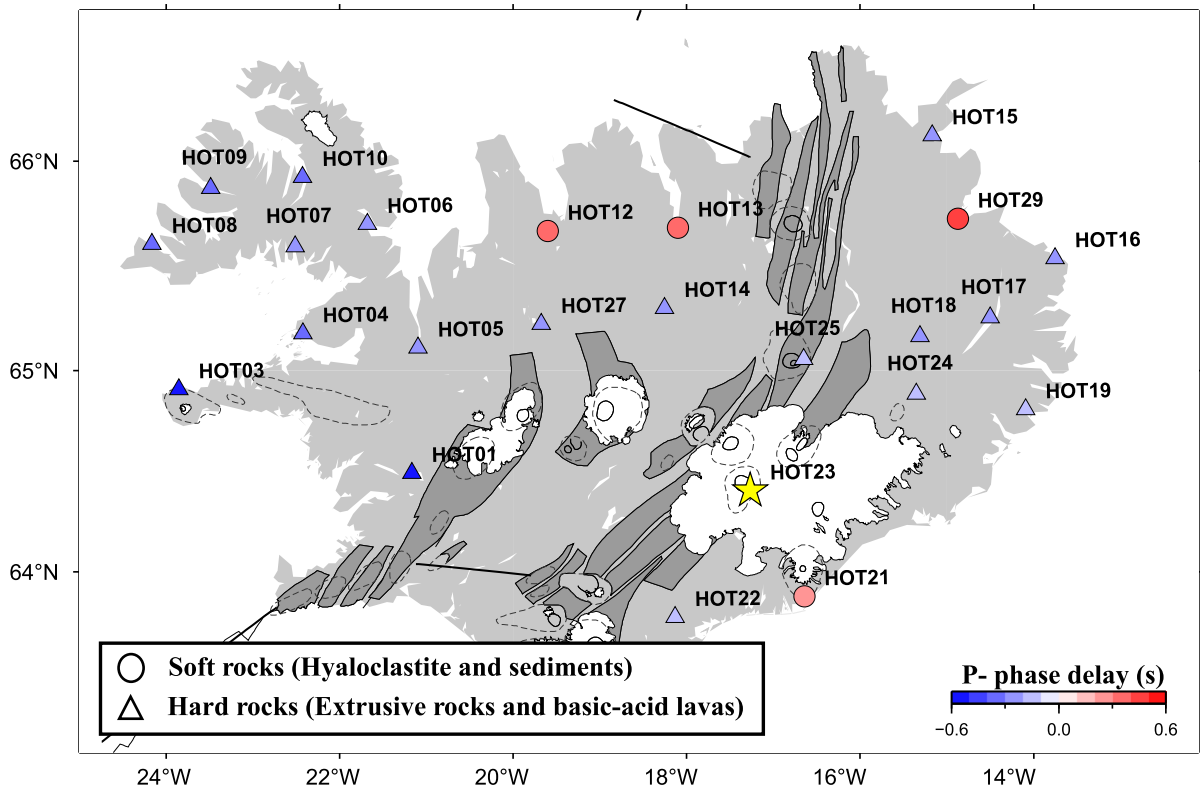


Figure 3

Map of the HOTSPOT stations superimposed on the rift zones of Iceland, describing the spatial variation of P-phase delay as estimated by VELEST. Different symbols represent different surface geology at each station site as seen in the legend. Station HOT23 is shown as a yellow star, since it was selected as the reference station. All other symbols are the same as in Fig. 1

times along a regular grid by utilizing the finite differences algorithm of Podvin and Lecomte (1991). A V_p/V_s ratio equal to 1.78 was assumed for the calculation of the S-wave travel times, which is consistent with the results of Allen et al. (2002) and Green et al. (2017) for the Icelandic crust. The resulting absolute locations of the 301 events have relatively well-constrained epicenters with average horizontal uncertainties of 3.87 km (± 3.67 km) and average RMS residual of 0.21 s (± 0.27 s). The vertical uncertainty of the absolute locations, however, was quite significant (typically larger than 4 km) for the majority of the events.

The epicenters form several clusters, some of them along the Bárðarbunga caldera and one elongated cluster between Bárðarbunga and Grimsvötn that partly coincides with the site of the Gjalp fissure (Fig. 4). In order to investigate the temporal variation

of the earthquake locations we plot in Fig. 5 the latitude of each location against the event origin time for the whole study period (29 September–12 October). Based on this diagram and the locations map, it can be clearly seen that shortly (~ 160 min) after the Bárðarbunga main event its aftershocks delineated the SW caldera rim of the volcano and then activity migrated to the SE of Bárðarbunga forming initially a small cluster of events. The next day (30 September) events started occurring at the same cluster and slowly migrated towards Grimsvötn along a SW direction, with some of them being located inside the Grimsvötn caldera. On 1 October the eruption broke through the ice and became subaerial, forming the 7 km long Gjalp fissure; seismicity during this day is concentrated around the fissure with few events also located near the Bárðarbunga caldera. The next few days events were occurring both near the fissure area

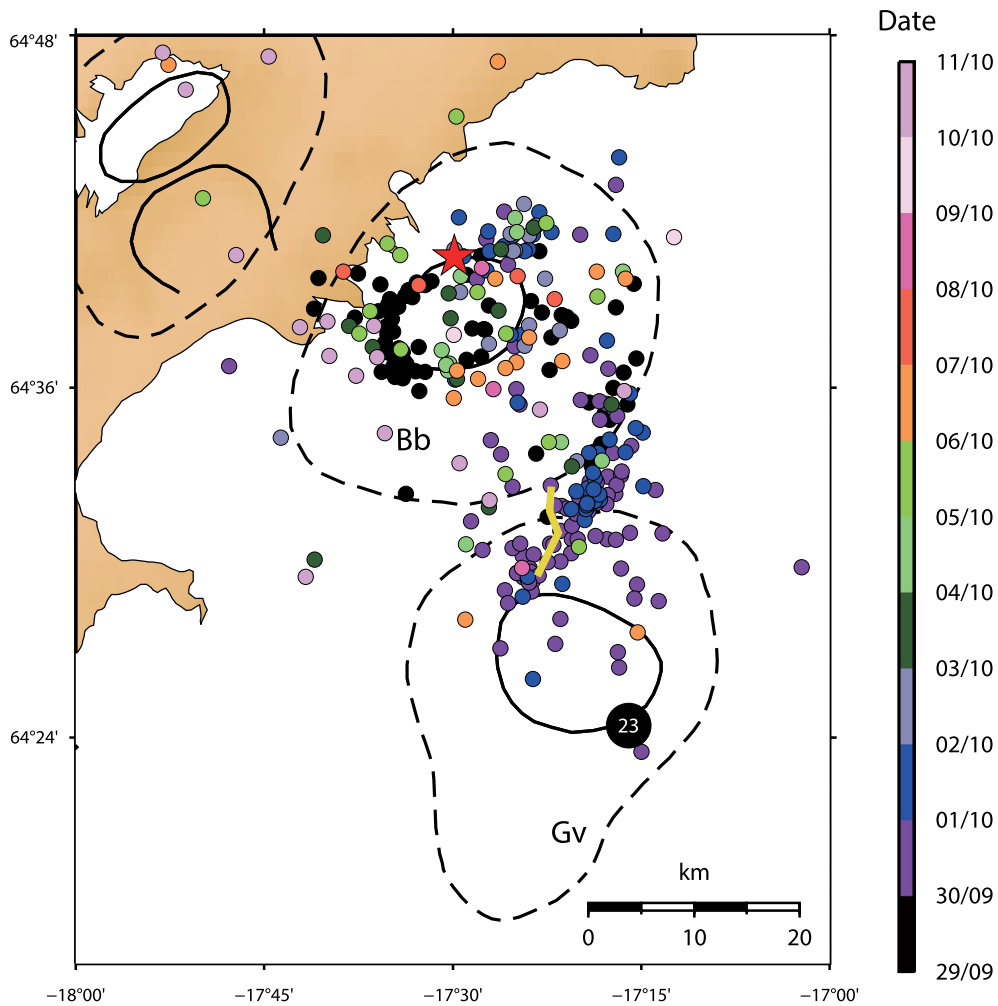


Figure 4

Map showing the absolute locations of 301 events that were identified during the 1996 Gjalp eruption and obtained by using NONLINLOC and the minimum 1D velocity model with station delays. Event locations are shown as dots having a color that follows the scale at the right of the plot, signifying the different days that the eruption was occurring. The red star represents the Bárðarbunga main event that occurred on 29 September (10:48 UTM). The thick yellow line corresponds to the Gjalp fissure. All other symbols are the same as in Fig. 1

and along the Bárðarbunga caldera, while towards the end of the study period (5–12 October) a small number of events was located in the Tungnafellsjökull volcanic system. The latter activity is consistent with InSAR observations of crustal deformation at Tungnafellsjökull during the same period that was interpreted as slip along pre-existing faults (Pagli et al. 2007).

We further employed the double-difference algorithm (Waldhauser and Ellsworth 2000), or HYPODD, in order to obtain more precise relative

locations. The algorithm adjusts the difference in hypocentral locations for pairs of earthquakes by minimizing their observed and theoretical travel time difference at each station. HYPODD can handle differential travel times calculated from both catalog observations and from waveform cross-correlation. We first calculated catalog differential travel times for pairs of earthquakes that were separated by a distance of less than 5 km. Cross-correlation differential travel times were also calculated for a tapered 2 s window around the picked P-phase and after

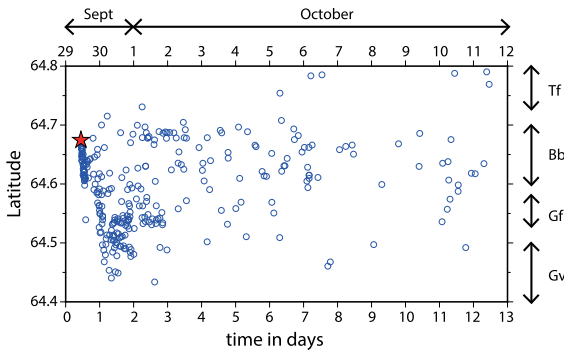


Figure 5

Diagram that shows the variation of NONLINLOC location latitude versus time for all the events. The red star represents the main Bárðarbunga earthquake that initiated the sequence. Lower x-axis gives absolute time while upper x-axis depicts calendar dates. Tf: Tungnafellsjökull, Bb: Bárðarbunga, Gf: Gjálp fissure, Gv: Grimsvötn

lowpass filtering the waveforms with a corner frequency of 5 Hz. Two waveforms were considered similar only if they exhibited a cross-correlation coefficient of 0.75 or higher. We utilized again the minimum 1D velocity model with a V_p/V_s ratio of 1.78 in order to calculate theoretical differential travel times. According to Waldhauser (2001) a two-step weighting scheme should be applied, where in the first step catalog differential times get a higher weight and in the second step they are down-weighted relative to the cross-correlation differential times. This scheme ensures that the relative position of each cluster is first constrained, before constraining the locations of close-by events within each cluster. HYPODD offers two ways in order to solve the linear system of double-difference equations, namely the LSQR (conjugate gradients) and SVD (singular value decomposition) method. SVD provides accurate estimates of uncertainties at the cost of being more computationally demanding as the number of events increases. Since the total number of our events does not exceed 301, we opted for using the SVD method for the relocation.

From the initial 301 events, HYPODD finally relocated 192 of them with horizontal relative uncertainties that do not exceed 1 km and RMS residuals of less than 0.2 s for the majority of the events (Fig. 6). Vertical relative uncertainties were found to be smaller than 1.2 km for the majority of the events (cf. Fig. 6). Figure 7 shows a map of the

relative locations obtained as a function of the hypocentral depth for each event. The general pattern seen in the absolute locations can be also observed here, with events clustered at the SW rim of the Bárðarbunga caldera and around the site of the Gjálp fissure. Figure 8 shows a depth cross-section across the Bárðarbunga caldera and two cross-sections along/across the elongated cluster in the Gjálp fissure. The majority of the events are located between 3 and 8 km depth (relative to sea level), with the latter depth being consistent with estimates of melt depth in NW Vatnajökull of 8–12 km (Gudmundsson et al. 2016; see also Fig. 1 of Hudson et al. 2017). Cross-section A–A' uses a width of 2.4 km in either side of the profile to project hypocenters on the vertical plane in order to allow a clearer view of their depth distribution, especially in the area near the SW caldera rim. The main event that preceded the eruption is relocated at 4 km depth in accordance with previous studies (Konstantinou et al. 2003; Tkalčić et al. 2009; Fichtner and Tkalčić 2010). Furthermore, the events that cluster at the rim of the caldera appear to become deeper along the SW direction. Table S2 in the supplementary material contains the relative locations and uncertainties for the 192 events relocated by HYPODD.

5. Moment Tensor Inversion

The Bárðarbunga main event has been studied in detail by several authors (Nettles and Ekström 1998; Konstantinou et al. 2003; Tkalčić et al. 2009; Fichtner and Tkalčić 2010) who concluded that its source is characterized by a large CLVD component and (like previous earthquakes at Bárðarbunga) it also exhibited a vertical T-axis. In this work, we also undertake a study of the source characteristics of the smaller earthquakes that followed after the Bárðarbunga main event. In order to do this we use a linear, time-domain inversion method described by Herrmann and Ammon (2002) for deriving the double-couple, deviatoric and full moment tensor solution of each event. The instrument response was first deconvolved and the horizontal components were rotated into radial and transverse with respect to the HYPODD location of each event. Waveforms were

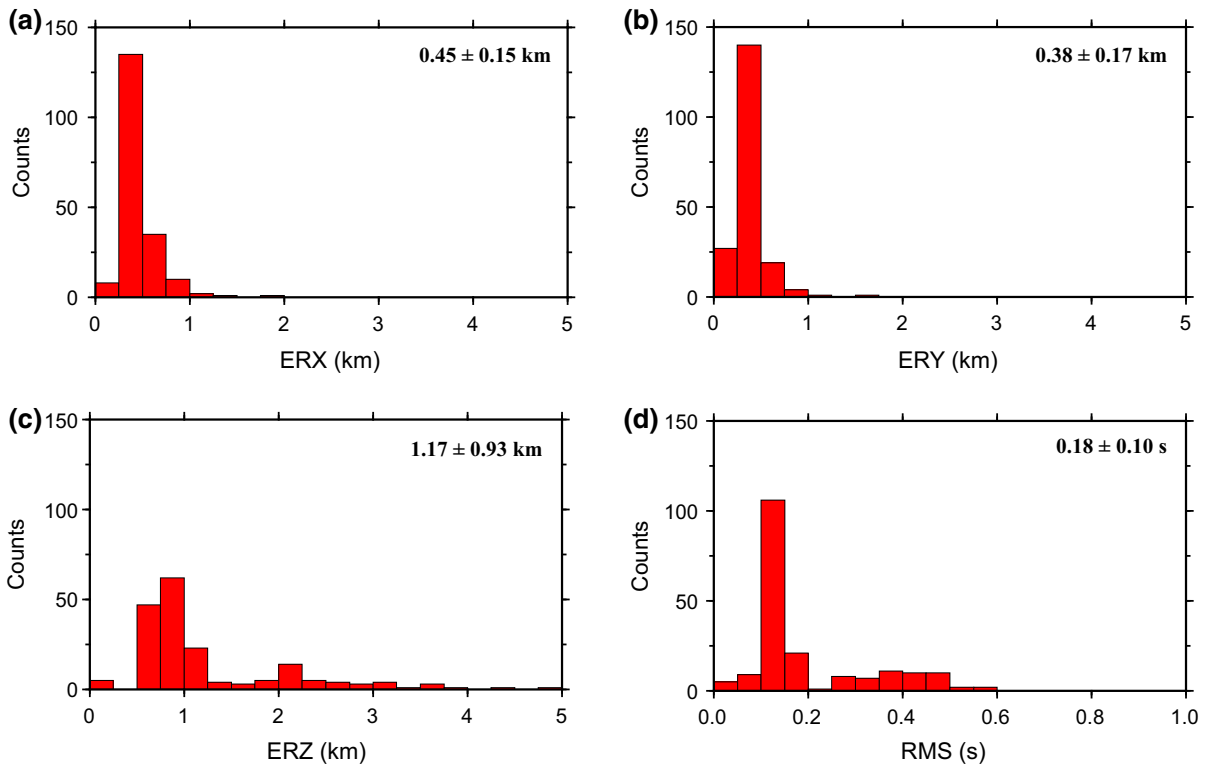


Figure 6

Histograms that represent the distribution of relative location uncertainties for the **a** X direction, **b** Y direction, **c** hypocentral depth, and **d** RMS residuals of all relocated events. The numbers at the upper right corner of each plot give the average and standard deviation of each distribution

filtered in the passband 0.05–0.08 Hz using a two-pole Butterworth filter. Green's functions were calculated by using the method of wavenumber integration and by employing the minimum 1D model for approximating the shallow crustal structure. Once computed, the Green's functions were filtered in the same way and aligned with the observed data. Inversions were performed for the depth range of 1–10 km with a step of 1 km and the moment tensor at the depth with the highest fit was considered as the final result.

We use the Bárðarbunga main event as a test case in order to ascertain whether the inversion approach described earlier can successfully reproduce its source characteristics. We indeed obtain a reverse faulting mechanism with almost vertical T-axis and a deviatoric moment tensor that is dominated by a CLVD component of 65% as found in previous studies (see Table 1). An intricate property of this

event is the lack of a significant isotropic component, despite the fact that it occurred in a volcano setting prior to an eruption (e.g., Tkalčić et al. 2009). It is well-known that models with more parameters (such as the full moment tensor) will fit the data better than models with fewer parameters (such the deviatoric moment tensor or a double-couple). However, this better fitting has to be confirmed statistically through the use of an F-test where its null hypothesis states that the variances of the fit of the two models are not significantly different. We perform the F-test for the Bárðarbunga main event following the procedure described in Templeton and Dreger (2006), who define the F statistic as the ratio of fit variance of the two models with each variance normalized by the number of uncorrelated data. In this way we find that at a confidence level of 95% the deviatoric moment tensor fits better than a double-couple solution, but the full moment tensor does not fit the data

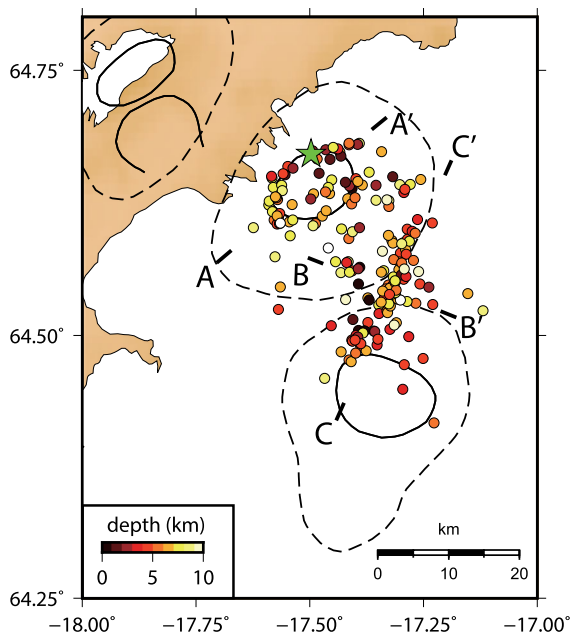


Figure 7

Map showing the relative locations of 192 events obtained by applying the HYPODD algorithm to catalog and cross-correlation differential travel time data. Event locations are shown as dots having a color that follows the scale at the lower left corner which signifies the hypocentral depth for each event. The green star represents the Bárðarbunga main event. Letters and dashes indicate the directions of depth cross-sections shown in Fig. 8

significantly better than the deviatoric one (i.e. the isotropic component is not significant).

Following the same procedure as for the Bárðarbunga main event, we inverted waveforms of 10 smaller events that contained energy in the lower frequencies (< 0.08 Hz). Three-component waveforms recorded at 4–6 stations were utilized for the majority of the events, providing a good azimuthal coverage around the NW part of Vatnajökull. The F-test at 95% confidence level concludes that the deviatoric moment tensor fits better the data than a simple double-couple solution and that the isotropic component is not statistically significant for all events. Tables 1 and 2 summarize the moment tensor and F-test results, while plots of observed and synthetic waveform fits for all events can be found in the supplementary material that accompanies this work (Figs. S1–S11). As it can be seen in Table 1 all of the studied events exhibit a CLVD component that ranges from 43 to 58%. While this component is statistically significant, there is uncertainty as to

whether it can be interpreted in terms of physical processes related to the volcanic activity. The reason for this is that large CLVD components may represent inversion artifacts generated by a combination of factors such as propagation effects not properly accounted for, limited number of nearby stations, or noise contamination (e.g., Panza and Saraò 2000). In our case all three of these factors are present: the 1D model we derived only crudely approximates the strongly heterogeneous Icelandic crust, most of our available stations are more than 100 km away, and the small magnitude of the events results in smaller recorded amplitudes that are susceptible to noise contamination. We therefore refrain from interpreting the CLVD component of the smaller events and rather focus our attention on the double-couple part of the solutions. Figure 9 depicts the epicentral locations of these events along with their corresponding beach balls. It can be seen that earthquakes located at the SW rim of the Bárðarbunga caldera display reverse focal mechanisms very similar to the main event and only the strike of the nodal planes appears to be varying. On the other hand, the events that are located near the Gjalp fissure exhibit mechanisms that are either strike-slip or have a large strike-slip component.

6. Ambient Noise Interferometry

Fichtner and Tkalčić (2010) performed a finite-fault inversion for the Bárðarbunga main event and concluded that in terms of kinematics the caldera moved downwards as one block, hence causing the rupture of an outward-dipping ring fault. However, such a caldera drop could only occur if some quantity of melt had left the magma chamber earlier than that. The authors speculated that a small subglacial eruption probably occurred prior to the Bárðarbunga main event but went on unnoticed. Analytical modeling of caldera collapse shows that for a deep (> 7 km) sill-like magma chamber, such as the one below Bárðarbunga, only a small percentage ($< 5\%$) of melt needs to evacuate the chamber in order to trigger a collapse (see Martí et al. 2000). There are two indications that such a scenario is plausible: (a) harmonic tremor started being recorded at HOT23 on 28

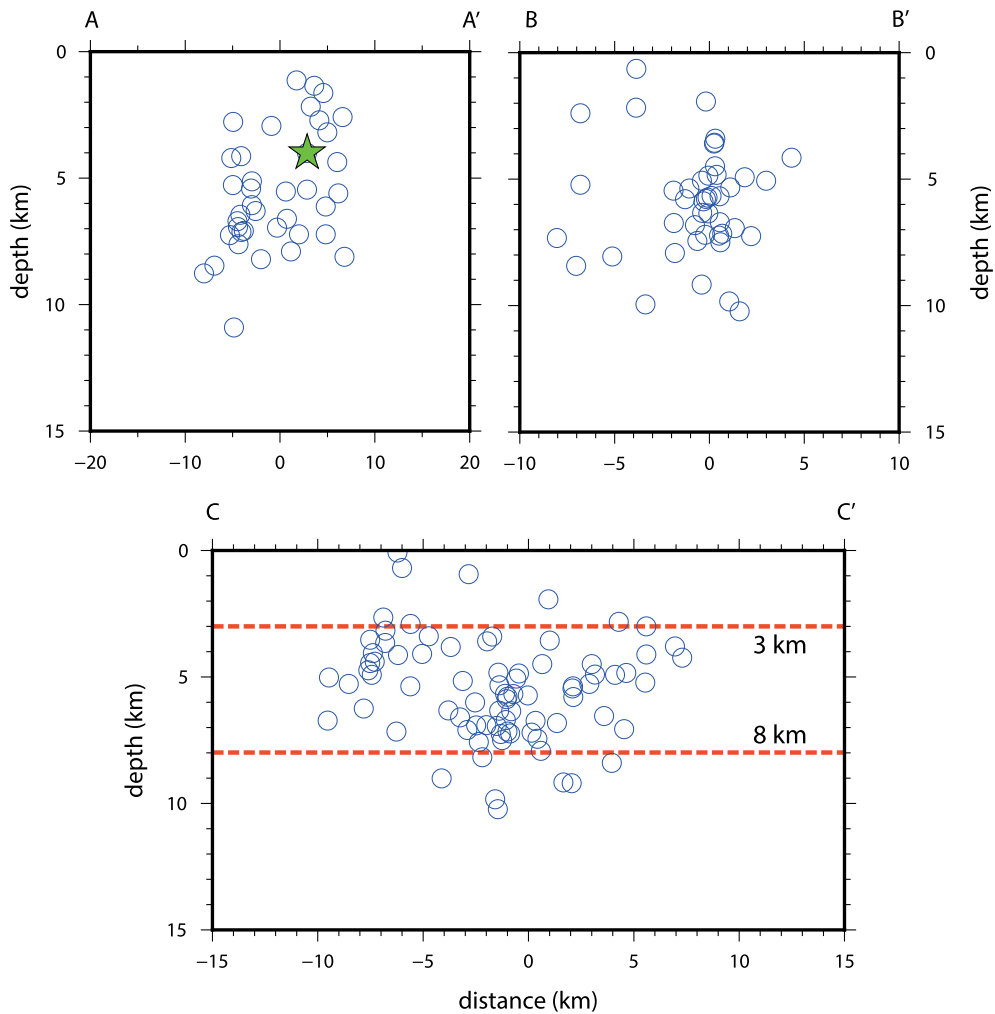


Figure 8

Cross-sections showing the distribution of hypocentral depths for the relocated events along the profiles given on the map of Fig. 7. The green star represents the Bárðarbunga main event. The dashed red lines in cross-section CC' delimit the depths that enclose 82% of the plotted hypocenters

September continuously up until 4.8 h prior to the Bárðarbunga main event (Konstantinou et al. 2000), and (b) Glynn and Konstantinou (2016) recently showed that about 8 days before the occurrence of the Bárðarbunga main event, higher frequencies (> 1 Hz) within the ambient seismic noise had disappeared at stations HOT23, HOT25 and HOT14. The authors interpreted these observations as resulting from high absorption losses due to melt reaching shallow depths.

Further evidence about the scenario of a small subglacial eruption prior to the Bárðarbunga main

event could be provided by a study of the relative velocity changes inferred from ambient noise interferometry (Brenner et al. 2008). In order to investigate this, we utilized the open-source Python package MSNoise (Lecocq et al. 2014) to calculate the noise cross-correlation functions (NCFs) and measure the relative velocity variations. Prior to the computation of the NCFs, a pre-processing was applied individually on the day-long vertical component traces of each station (Bensen et al. 2007). The data were initially bandpass filtered between 0.01 and 4 Hz, demeaned, tapered and down-sampled to

Table 1

Source parameters of the main Bárðarbunga earthquake and 10 other events that occurred afterwards

Event	Date	Origin Time	Lat (N)	Long (E)	Z (km)	Mw	Strike	Dip	Rake	% DC	% CLVD
Main event	29/09	10:48:16.17	64.6713	-17.4972	4	5.6	288	57	98	35.00	65.00
1	29/09	12:47:15.81	64.6303	-17.5731	6	4.3	297	60	102	43.37	56.63
2	29/09	13:21:27.31	64.6152	-17.5662	10	3.9	312	50	107	41.67	58.33
3	29/09	13:18:15.44	64.6117	-17.5690	4	4.1	87	66	81	48.48	51.52
4	29/09	13:39:14.73	64.6063	-17.5646	9	4.1	337	73	83	47.85	52.15
5	01/10	05:07:47.58	64.5917	-17.4142	6	4.2	280	45	87	52.04	47.96
6	30/09	09:07:25.23	64.4846	-17.4311	2	3.7	15	89	-161	50.11	49.89
7	30/09	10:37:08.70	64.5049	-17.3927	6	3.7	60	79	-26	56.64	43.36
8	30/09	18:46:39.73	64.5351	-17.3137	4	4.2	317	67	-87	59.95	40.05
9	30/09	16:22:00.94	64.5477	-17.3268	9	3.8	17	90	-159	49.36	50.64
10	30/09	05:45:48.24	64.5815	-17.2894	7	3.7	165	89	8	56.77	43.23

Column Z signifies the depth inferred from the moment tensor inversion

10 Hz. The data were then clipped to 3 times the root-mean-square amplitude for time domain normalization and spectrally whitened. NCFs were computed in 30-min windows for maximum time lags of ± 200 s, were linearly stacked for each day, and then the daily NCFs were stacked over 2-day long moving windows. All daily NCFs were stacked over the whole recording period in order to build a reference NCF. The Moving-Window Cross-Spectral (MWCS) method (Clarke et al. 2011) was applied to monitor the relative velocity variation with time, by measuring the temporal dephasing between the daily

NCF and the reference NCF. In particular, the MWCS method consists of two main steps (for a detailed description of the method, see Clarke et al. 2011 and Lecocq et al. 2014): first, the time delay (dt)

Table 2

Summary of the *F*-test results for assessing the different source types of the studied events

Event	F-test result		
	F_{DC-DEV}	$F_{DEV-ISO}$	Critical value
Main event	1.73	1.00	1.29
1	1.95	1.03	1.28
2	1.70	1.02	1.28
3	1.78	1.08	1.31
4	2.10	1.00	1.28
5	1.73	1.00	1.28
6	1.76	0.96	1.49
7	1.85	1.00	1.58
8	1.78	1.06	1.36
9	1.58	0.97	1.49
10	2.51	1.02	1.43

Column F_{DC-DEV} signifies the variance ratio of double-couple (DC) to deviatoric moment tensor, while column $F_{DEV-ISO}$ the same ratio for deviatoric to full moment tensor. These values are then compared to the critical value obtained from statistical tables for a confidence level of 95%

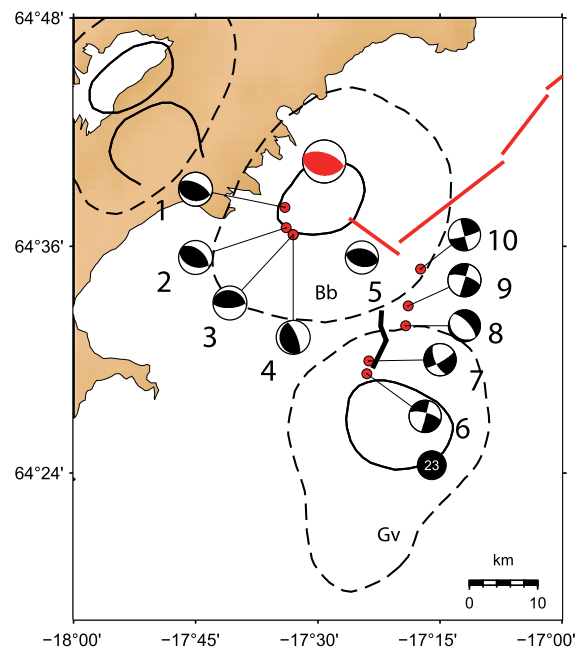


Figure 9

Map showing the locations (red dots) and focal mechanisms of events whose moment tensor was derived from waveform inversion (event numbers are the same as in Table 2). The red beach ball belongs to the Bárðarbunga main event. The black thick line is the Gjalp fissure that developed on the ice after the eruption reached the surface of the glacier (after Gudmundsson et al. 1997). The red thick lines are the segments of the dike intrusion during the 2014–2015 Bárðarbunga–Holuhraun eruption (after Sigmundsson et al. 2015)

between the current day's NCF and the reference NCF is measured at different lag times (t) within a series of overlapping windows at the coda part of the NCFs. Measurement points with dt greater than ± 0.1 s, a coherence of less than 0.65 and an error greater than 0.1 s were rejected. In the second step, a line is fitted to the remaining dt measurements as a function of t , weighted by the error estimates of each dt (weighted linear regression). Under the assumption of a homogeneous relative velocity perturbation in the medium (e.g., Ratdomopurbo and Poupinet 1995), the equation $dv/v = -dt/t$ can be used to calculate the relative velocity variation.

Ambient noise interferometry relies on the cross-correlation of continuous noise recordings for pairs of stations that are usually selected based on a number of criteria. In our case these criteria have to do with (a) data availability, (b) the path that connects the two stations which should pass through the Bárðarbunga caldera, and (c) the total length of this path which should be as small as possible in order to increase the chances of detecting velocity variations. Considering that station HOT26 was not in operation during the study period and that HOT27 as well as HOT28 contained large data gaps, we focused our attention on the pair HOT23–HOT14 that satisfied all three criteria. Figures S12–S13 in the supplementary material depict spectrograms of seismic noise at the two stations, where it can be seen that most energy is concentrated between the second microseism band (0.1–1 Hz). The dv/v measurements were performed in the frequency band between 0.5 and 1 Hz, using 2-day moving window stacks of the NCFs. We further calculated the depth sensitivity of emergent Rayleigh waves comprising seismic noise for the frequency of 0.5 Hz by utilizing the minimum 1D velocity model derived in Sect. 3 and calculating shear wave velocities using a V_p/V_s ratio equal to 1.78 (Fig. 10). It can be seen that any velocity variations in this frequency band should correspond to medium changes up to a depth of 4 km.

Figure 11 shows the relative velocity variations for this pair of stations from 31 July until 11 October. A trend of increasing relative velocity can be seen from 9 until 28 September probably as a result of the buildup of overpressure inside the Bárðarbunga magma chamber. In order to investigate whether this

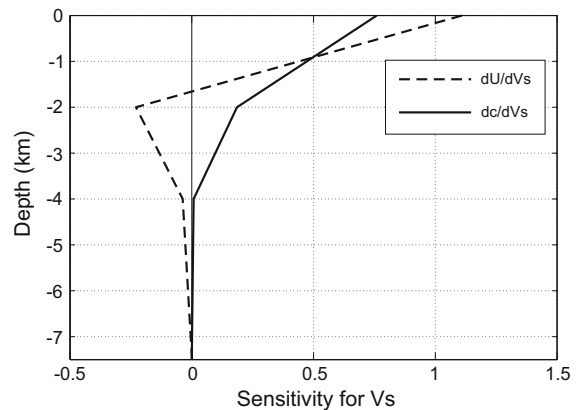


Figure 10
Depth sensitivity kernel of Rayleigh wave for group (dashed line) and phase (solid line) velocity for the frequency of 0.5 Hz (see text for more details)

trend is statistically significant, we applied linear regression and performed a t test for determining the significance of the slope and intercept of the fitted line at 95% confidence level. In both cases we find that the p value is in the order of 0.01 which is smaller than 0.05, hence the null hypothesis of no significant trend can be rejected. On 28 September, about 1 day before the occurrence of the Bárðarbunga main event, a sharp decrease of relative velocity occurs from + 0.06% to negative values. While this drop could be interpreted as a sign of magma ascent, it also coincides with the onset of harmonic tremor that was recorded at HOT23. Previous studies (e.g., Ballmer et al. 2013) have shown that volcanic tremor may affect the calculation of relative velocity values in a manner that they may no longer represent real medium changes. Another point that deserves attention is the fact that the path of HOT23–HOT14 also crosses the Tungnafellsjökull volcanic system where a handful of earthquakes were located after the Gjalp eruption. This earthquake activity was shown to be the result of unclamping of pre-existing faults triggered by magma withdrawal and subsidence at Bárðarbunga (Pagli et al. 2007; Parks et al. 2017). It is therefore unlikely that the increase in relative velocities we observed were due to localized inflation beneath Tungnafellsjökull.

These considerations suggest that only this increase in relative velocity during 9–28 September can be interpreted as a robust precursory feature. The

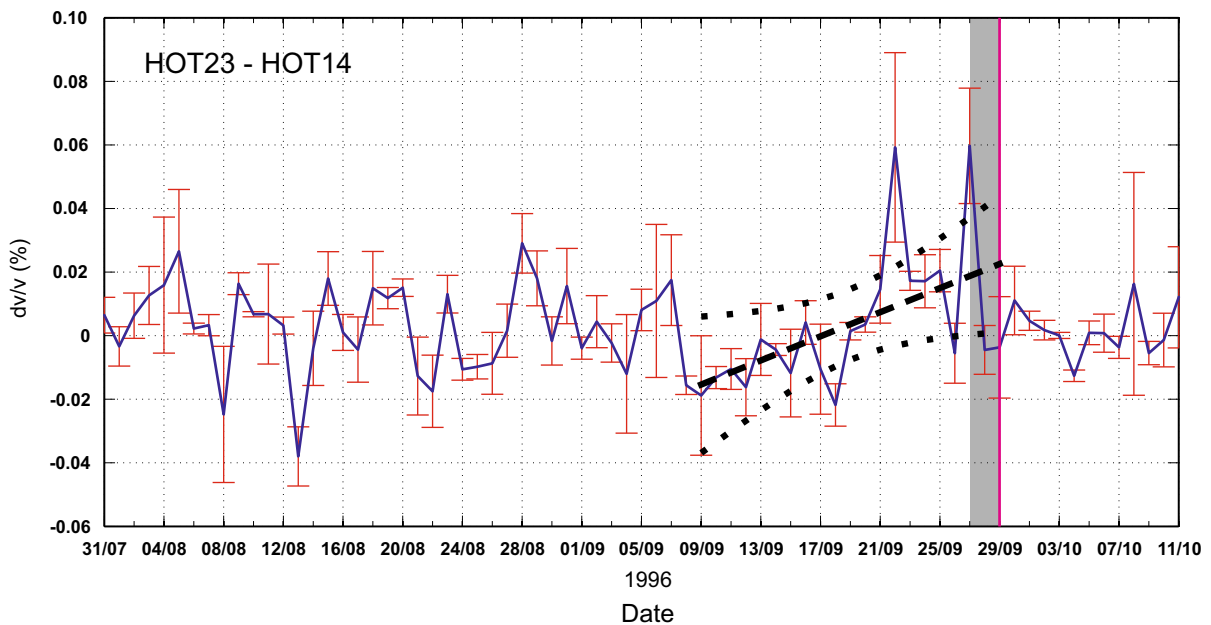


Figure 11

Relative seismic velocity variations, dv/v , for station pair HOT14–HOT23. Error bars indicate the error in the measurements. The vertical line in magenta marks the occurrence of the 29 September M_w 5.6 earthquake, while the dashed black line shows a linear regression line fitted to the dv/v values for a period of 20 days before the occurrence of the earthquake. The black dotted curves represent the 95% confidence limits of the regression (see text for more details). The gray shaded area highlights the period where relative velocity drops from + 0.06% to negative values and also coincides with the onset of volcanic tremor at HOT23

buildup of overpressure and subsequent occurrence of harmonic tremor point to the possibility of a small subglacial eruption that may have occurred at Bárðarbunga. This resulted in the removal of some quantity of melt from its magma chamber, which in turn induced the caldera drop and the rupture of its ring fault. Similar small subglacial eruptions might have occurred prior to the other anomalous Bárðarbunga earthquakes analyzed by Nettles and Ekström (1998). It is highly likely that these eruptions went unnoticed as well, firstly because they did not break through the ice, and secondly because regional networks in past decades had very limited capabilities to detect weak tremor signals or microseismicity in such a remote area as NW Vatnajökull.

7. Discussion

One distinct difference between the seismicity observed during the 1996 Gjalp and the 2014–2015

Bárðarbunga–Holuhraun eruption was the opposite sense of motion for the events around the Bárðarbunga caldera rim. During the 2014–2015 eruption earthquakes clustered in the NE and SE parts of the caldera exhibited normal faulting with large CLVD components (Riel et al. 2015). On the contrary, during the 1996 eruption events clustered in the NW and SW parts of the caldera and their moment tensor solutions indicate reverse faulting (cf. Fig. 9). One way to reconcile this difference is to accept that the two groups of events nucleated along ring faults of varying dip (see also Fig. 6c of Gudmundsson et al. 2016): during 1996 the ring fault was dipping outwards, while during 2014–2015 it was dipping inwards. The relocated epicenters along the caldera rim support the existence of a ring fault as the nucleation site of the Bárðarbunga main event, while moment tensors of its aftershocks reveal a rather complicated geometry for this fault as judged by the rotation of their nodal planes along the caldera rim (cf. Fig. 9).

The migration of seismic activity from Bárðarbunga to the area of the Gjalp fissure was much less spectacular than the migration of events during the 2014–2015 dike intrusion. However, the mechanics of faulting during the intrusion of magma seems to be in both cases similar. In the 2014–2015 dike intrusion, Ágústsdóttir et al. (2016) found that the majority of the earthquakes along the dike path were located within a narrow zone at 5–7 km depth. The authors suggested that the rocks shallower than 5 km were inherently weak due to repeated rifting episodes, therefore they could not sustain brittle failure. On the contrary, the depths between 5 and 7 km signify the brittle-ductile boundary for the Icelandic crust and the differential stresses in this zone are expected to be the highest. Analysis of the focal mechanisms of events along the dike intrusion showed that the majority of them exhibited strike-slip faulting and that no event had any significant isotropic component. The authors concluded that the opening of the dike was probably aseismic and that the strike-slip motion released the accumulated strain deficit along the dike path. Even though the number of earthquakes recorded during the 1996 eruption is orders of magnitude smaller than that of 2014–2015, our results also give a hint of similar processes along the Gjalp fissure. The majority of the relocated earthquakes occur at depths shallower than 8 km and deeper than 3 km (relative to the sea level), suggesting that the upper part of the dike that reached the rock-ice interface was indeed aseismic. The available focal mechanisms exhibit strike-slip components and insignificant volumetric source changes (cf. Table 2), pointing to aseismic opening of the dike beneath the fissure as well as strain release in the form of strike-slip faulting. These results agree well with the conclusion of Spaans and Hooper (2018) that the accumulated strain due to plate spreading in the south of the 2014–2015 dike path had already been released by previous eruptions such as the 1996 Gjalp.

Figure 12 depicts a simplified cartoon that describes the subsurface features beneath the two central volcanoes, the kinematics of faults, and the magma path according to the results of this and previous studies. The depth of the shallow magma chamber beneath Bárðarbunga is constrained by the depth distribution of seismicity between 8 and 12 km

(Gudmundsson et al. 2016; Hudson et al. 2017) and also by the results of our relocation. The depth and shape of the magma chamber beneath Grimsvötn has been inferred from tomographic inversion of earthquake travel times (Alfaro et al. 2007). The starting point of the Gjalp eruption was the pressurization of the magma chamber beneath Bárðarbunga, as has been demonstrated by the gradual increase of the relative seismic velocities. The subsequent occurrence of volcanic tremor probably signified the extrusion of some amount of melt from the chamber that gave rise to a small subglacial eruption that went on unnoticed. After this the roof of the Bárðarbunga magma chamber drops and this causes the rupture of the outward dipping ring fault that produced the main event and its aftershocks. The caldera drop induces further pressure increase which leads to the melt being squeezed out of the magma chamber, migrating laterally underneath the area of the Gjalp fissure. The magma overpressure and stresses due to plate spreading open a dike and deformation along this dike causes earthquakes with substantial strike-slip components. The dike tip reaches the interface between the rock and the icecap and the subglacial eruption starts, at first melting the ice and later reaching the free surface as described in Gudmundsson et al. (1997). At this point it should be noted that earthquakes at the SW tip of the Gjalp fissure were occurring very close to the Grimsvötn shallow magma chamber (cf. Fig. 8 cross-section C–C'). Numerical models support the possibility of shared magma pathways between Bárðarbunga and Grimsvötn, both in terms of the existence of a tensile-stress concentration zone between the two volcanoes, and in terms of the orientation of the principal maximum stress axis (Gudmundsson and Andrew 2007). It is therefore conceivable that these earthquakes might have created fractures that could allow melt from Grimsvötn to leak towards the Gjalp fissure.

8. Conclusions

We reanalyzed the seismicity recorded during the 1996 Gjalp eruption in Iceland, for the purpose of better understanding the physical mechanism of the eruption by combining our results with those from

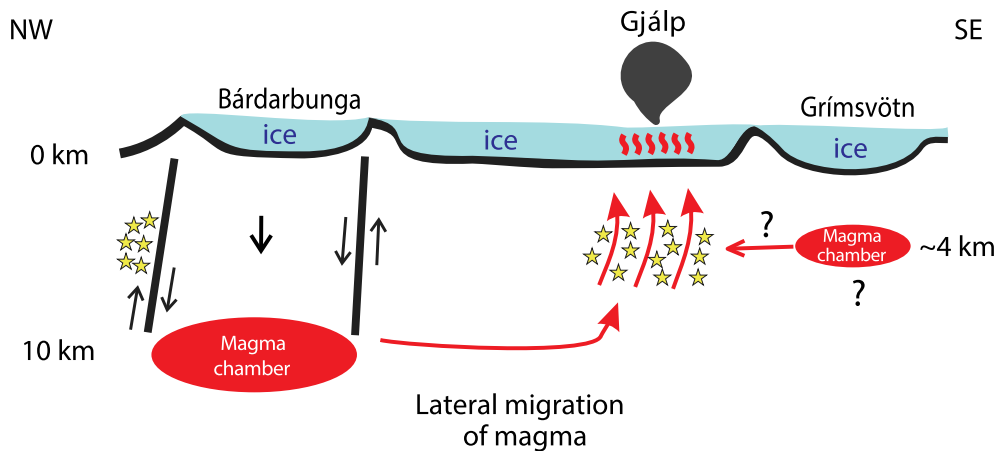


Figure 12

Cartoon (not to scale) illustrating the different volcano-tectonic elements beneath the area of NW Vatnajökull where Bárðarbunga and Grímsvötn volcanoes are situated. Thick black lines indicate faults and black arrows give a sense of the fault/block kinematics. Thick red arrows show the possible movement of magma from the corresponding magma chambers (see text for more details). Stars represent earthquake activity at the rim of the Bárðarbunga caldera and beneath the Gjalp fissure

previous studies. The main conclusions of this work can be summarized as follows:

1. In total 301 events were identified that formed two main clusters, one at Bárðarbunga caldera and the other at the site of the Gjalp fissure. Precise relative locations obtained with HYPODD showed that the maximum depth of these events did not exceed 10 km as found in previous studies for this area. Relative locations also showed that the epicenters of the aftershocks of the Bárðarbunga main event delineate its caldera rim. Seismic activity then migrated within a few hours to the site of the Gjalp fissure, while some earthquakes were also located at the neighboring Tungnafellsjökull volcano.
2. Moment tensor inversion results showed that the events at the rim of the Bárðarbunga caldera exhibited reverse faulting. This could be interpreted as faulting along a ring fault whose segments exhibit varying strike and dip. Events that were located near the Gjalp fissure exhibited strike-slip focal mechanisms. These events most likely signified the release of strain along the path of magma. All the events whose moment tensors were derived showed statistically insignificant isotropic components. CLVD components, while statistically significant, are more likely the result

of unmodeled propagation effects, the limited number of available stations and the presence of noise.

3. Prior to the Bárðarbunga main event (9–28 September) ambient noise interferometry revealed a robust increase in relative seismic velocity along the path that traverses the Bárðarbunga caldera, which may correspond to the pressurization of its magma chamber. On 28 September harmonic tremor starts being recorded by the closest station to the eruption site, possibly signifying the occurrence of a small subglacial eruption. Such an eruption could have caused a small quantity of melt to leave the magma chamber leading to the collapse of its roof, the rupture of the ring fault, and eventually to the lateral migration of magma towards the Gjalp fissure.

Acknowledgements

The first author would like to thank the Ministry of Science and Technology of Taiwan (MOST; Grant no.: MOST107-2116-M-008-015) for the financial support of this study in the form of a research grant. Ika Wahyu Utami held a scholarship from the School of Earth Sciences while studying for a graduate

degree at National Central University. The waveforms analyzed in this study are freely available from the IRIS database. We would like to thank the Editor Ben Edwards for handling our manuscript, as well as Tim Greenfield and an anonymous reviewer for their constructive comments.

Publisher's Note Springer Nature remains neutral with regard to jurisdictional claims in published maps and institutional affiliations.

REFERENCES

- Ágústsdóttir, T., Woods, J., Greenfield, T., Green, R. G., White, R. S., Winder, T., et al. (2016). Strike-slip faulting during the 2014 Bárðarbunga–Holuhraun dike intrusion, central Iceland. *Geophysical Research Letters*, *43*, 1495–1503. <https://doi.org/10.1002/2015GL067423>.
- Alfaro, R., Brandsdóttir, B., Rowlands, D. P., White, R. S., & Gudmundsson, M. T. (2007). Structure of the Grimsvötn central volcano under the Vatnajökull icecap, Iceland. *Geophysical Journal International*, *168*, 863–876. <https://doi.org/10.1111/j.1365-246X.2006.03238>.
- Allen, R. M., et al. (2002). Imaging the mantle beneath Iceland using integrated seismological techniques. *Journal of Geophysical Research*, *107*(B12), 2325.
- Ballmer, S., Wolfe, C. J., Okubo, P. G., Haney, M. M., & Thurber, C. H. (2013). Ambient seismic noise interferometry in Hawaii reveals long-range observability of volcanic tremor. *Geophysical Journal International*, *194*, 512–523. <https://doi.org/10.1093/gji/ggt112>.
- Bensen, G. D., Ritzwoller, M. H., Barmin, M. P., Levshin, A. L., Lin, F., Moschetti, M. P., et al. (2007). Processing seismic ambient noise data to obtain reliable broad-band surface wave dispersion measurements. *Geophysical Journal International*, *169*(3), 1239–1260.
- Bjarnason, I. T. (2014). Earthquake sequence 1973–1976 in Bárðarbunga volcano: seismic activity leading up to eruptions in the NW-Vatnajökull area. *Jökull*, *64*, 61–82.
- Bjarnason, I. T., Menke, W., Flovenz, O. G., & Caress, D. (1993). Tomographic image of the Mid-Atlantic plate boundary in southwestern Iceland. *Journal of Geophysical Research*, *98*, 6607–6622.
- Björnsson, H. (1988). *Hydrology of ice caps in volcanic regions*. Reykjavík: Societas Scientiarum Islandica, University of Iceland.
- Björnsson, H., & Einarsson, P. (1990). Volcanoes beneath Vatnajökull Iceland: evidence from radio echo-sounding, earthquakes and jökulhlaups. *Jökull*, *40*, 147–167.
- Björnsson, H., & Gudmundsson, M. T. (1993). Variations in thermal outputs of the subglacial Grimsvötn caldera, Iceland. *Geophysical Research Letters*, *20*, 2127–2130.
- Brenguier, F., Shapiro, N. M., Campillo, M., Ferrazzini, V., Duputel, Z., Coutant, O., et al. (2008). Towards forecasting volcanic eruptions using seismic noise. *Nature Geosci.*, *1*, 126–130. <https://doi.org/10.1038/ngeo104>.
- Clarke, D., Zaccarelli, L., Shapiro, N. M., & Brenguier, F. (2011). Assessment of resolution and accuracy of the Moving Window Cross Spectral technique for monitoring crustal temporal variations using ambient seismic noise. *Geophysical Journal International*, *186*(2), 867–882. <https://doi.org/10.1111/j.1365-246X.2011.05074.x>.
- Einarsson, P., Brandsdóttir, B., Gudmundsson, M. T., & Björnsson, H. (1997). Center of the Iceland hotspot experiences volcanic unrest. *Eos, Transactions American Geophysical Union*, *78*, 374–375.
- Fichtner, A., & Tkalčić, H. (2010). Insights into the kinematics of a volcanic caldera drop: Probabilistic finite-source inversion of the 1996 Bárðarbunga, Iceland, earthquake. *Earth and Planetary Science Letters*, *297*(3–4), 607–615. <https://doi.org/10.1016/j.epsl.2010.07.013>.
- Glynn, C. C., & Konstantinou, K. I. (2016). Reduction of randomness in seismic noise as a short-term precursor to a volcanic eruption. *Scientific Reports*, *6*, 37733. <https://doi.org/10.1038/srep37733>.
- Green, R. G., Priestley, K., & White, R. S. (2017). Ambient noise tomography reveals upper crustal structure of Icelandic rifts. *Earth and Planetary Science Letters*, *466*, 20–31. <https://doi.org/10.1016/j.epsl.2017.02.039>.
- Gudmundsson, A., & Andrew, R. E. B. (2007). Mechanical interaction between volcanoes in Iceland. *Geophysical Research Letters*, *34*, L10310. <https://doi.org/10.1029/2007GL029873>.
- Gudmundsson, M. T., & Högnadóttir, T. (2007). Volcanic systems and calderas in the Vatnajökull region, central Iceland: Constraints on crustal structure from gravity data. *Journal of Geodynamics*, *43*, 153–169. <https://doi.org/10.1016/j.jog.2006.09.015>.
- Gudmundsson, A., Lecoeur, N., Mohajeri, N., & Thordarson, T. (2014). Dike emplacement at Bárðarbunga, Iceland, induces unusual stress changes, caldera deformation, and earthquakes. *Bulletin of Volcanology*, *76*, 869. <https://doi.org/10.1007/s00445-014-0869-8>.
- Gudmundsson, M. T., Sigmundsson, F., & Björnsson, H. (1997). Ice-volcano interaction of the 1996 Gjalp subglacial eruption. *Vatnajökull, Iceland, Nature*, *389*, 954–957.
- Gudmundsson, M. T., et al. (2016). Gradual caldera collapse at Bárðarbunga volcano, Iceland, regulated by lateral magma outflow. *Science*, *353*, aaf8988. <https://doi.org/10.1126/science.aaf8988>.
- Herrmann, R. B., & Ammon, C. J. (2002). *Computer programs in seismology—source inversions: User's manual, report*. St Louis Mo: St Louis University.
- Hudson, T. S., White, R. S., Greenfield, T., Ágústsdóttir, T., Brisbourne, A., & Green, R. G. (2017). Deep crustal melt plumbing of Bárðarbunga volcano, Iceland. *Geophysical Research Letters*, *44*, 8785–8794. <https://doi.org/10.1002/2017GL074749>.
- Kissling, E. (1995). Program VELEST user's guide—short introduction. Institute of Geophysics, ETH Zurich.
- Kissling, E., Ellsworth, W. L., Eberhart-Phillips, D., & Kradolfer, U. (1994). Initial reference models in local earthquake tomography. *Journal of Geophysical Research*, *99*, 19635–19646.
- Konstantinou, K. I. (2002). Deterministic non-linear source processes of volcanic tremor signals accompanying the 1996

- Vatnajökull eruption, central Iceland. *Geophysical Journal International*, 148, 663–675.
- Konstantinou, K. I., Kao, H., Lin, C.-H., & Liang, W.-T. (2003). Analysis of broad-band regional waveforms of the 1996 September 29 earthquake at Bárðarbunga volcano, central Iceland: investigation of the magma injection hypothesis. *Geophysical Journal International*, 154, 134–145.
- Konstantinou, K. I., Nolet, G., Morgan, W. J., Allen, R. M., & Pritchard, M. J. (2000). Seismic phenomena associated with the 1996 Vatnajökull eruption, central Iceland. *Journal of Volcanology and Geothermal Research*, 102, 169–187.
- Larsen, G. (2002). A brief overview of eruptions from ice-covered and ice-capped volcanic systems in Iceland during the past 11 centuries: Frequency, periodicity and implications. *Geological Society, London, Special Publications*, 202, 81–90. <https://doi.org/10.1144/gsl.sp.2002.202.01.05>.
- Lecocq, T., Caudron, C., & Brenguier, F. (2014). MSNoise, a python package for monitoring seismic velocity changes using ambient seismic noise. *Seismological Research Letters*, 85(3), 715726. <https://doi.org/10.1785/0220130073>.
- Lomax, A., & Curtis, A. (2001). Fast, probabilistic earthquake location in 3D models using Oct-Tree importance sampling. *Geophysical Research Abstracts* 3.
- Lomax, A., Michelini, A., & Curtis, A. (2009). Earthquake location, direct, global-search methods, in complexity. In *Encyclopedia of complexity and system science*, Part 5. Springer, New York, pp. 2449–2473, <https://doi.org/10.1007/978-0-387-30440-3>.
- Lomax, A., Virieux, J., Volant, P., & Berge-Thierry, C., (2000). Probabilistic earthquake location in 3D and layered models. In: Thurber, R. (Eds.), *Advances in seismic event location*, pp. 101–134.
- Martí, J., Folch, A., Neri, A., & Macedonio, G. (2000). Pressure evolution during explosive caldera-forming eruptions. *Earth and Planetary Science Letters*, 175, 275–287.
- Nettles, M., & Ekström, G. (1998). Faulting mechanism of anomalous earthquakes near Bárðarbunga Volcano, Iceland. *Journal of Geophysical Research*, 103(B8), 17973–17983.
- Pagli, C., Sigmundsson, F., Pedersen, R., Einarsson, P., Árnadóttir, T., & Feigl, K. L. (2007). Crustal deformation associated with the 1996 Gjalp subglacial eruption, Iceland: InSAR studies in affected areas adjacent to the Vatnajökull ice cap. *Earth and Planetary Science Letters*, 259, 24–33. <https://doi.org/10.1016/j.epsl.2007.04.019>.
- Panza, G. F., & Saraò, A. (2000). Monitoring volcanic and geothermal areas by full seismic moment tensor inversion: are non-double-couple components always artifacts of modeling? *Geophysical Journal International*, 143, 353–364.
- Parks, M. M., et al. (2017). Evolution of deformation and stress changes during the caldera collapse and dyking at Bárðarbunga, 2014–2015: Implication for triggering of seismicity at nearby Tungnafellsjökull volcano. *Earth and Planetary Science Letters*, 462, 212–223. <https://doi.org/10.1016/j.epsl.2017.01.020>.
- Podvin, P., & Lecomte, I. (1991). Finite difference computation of traveltimes in very contrasted velocity models: a massively parallel approach and its associated tools. *Geophysical Journal International*, 105, 271–284.
- Pritchard M. J. (2000). A seismological study of the mantle beneath Iceland, PhD thesis, University of Durham.
- Ratdomopurbo, A., & Poupinet, G. (1995). Monitoring a temporal change of seismic velocity in a volcano: Application to the 1992 eruption of Mt. Merapi (Indonesia). *Geophysical Research Letters*, 22(7), 775–778. <https://doi.org/10.1029/95gl00302>.
- Riel, B., Milillo, P., Simons, M., Lundgren, P., Kanamori, H., & Samsonov, S. (2015). The collapse of Bárðarbunga caldera, Iceland. *Geophysical Journal International*, 202, 446–453. <https://doi.org/10.1093/gji/ggv157>.
- Ruch, J., Wang, T., Xu, W., Hensch, M., & Jónsson, S. (2016). Oblique rift opening revealed by recurring magma injection in central Iceland. *Nature Communications*, 7, 12352. <https://doi.org/10.1038/ncomms12352>.
- Shen, Y., Solomon, S. C., Bjarnason, I. T., & Wolfe, C. J. (1998). Seismic evidence for a lower-mantle origin of the Iceland plume. *Nature*, 395, 62–65.
- Sigmundsson, F., et al. (2015). Segmented lateral dyke growth in a rifting event at Bárðarbunga volcanic system, Iceland. *Nature*, 517, 191. <https://doi.org/10.1038/nature14111>.
- Spaans, K., & Hooper, A. (2018). Insights into the stress field around Bárðarbunga volcano from the 2014/2015 Holuhraun rifting event. *Journal of Geophysical Research Solid Earth*, 123, 3238–3249. <https://doi.org/10.1002/2017JB015274>.
- Templeton, D. C., & Dreger, D. S. (2006). Non-double-couple earthquakes in the Long Valley volcanic region. *Bulletin of the Seismological Society of America*, 96, 69–79. <https://doi.org/10.1785/0120040206>.
- Thordarson, T., & Larsen, G. (2007). Volcanism in Iceland in historical times: Volcano types, eruption styles and eruptive history. *Journal of Geodynamics*, 43, 118–152. <https://doi.org/10.1016/j.jog.2006.09.005>.
- Tkalčić, H., Dreger, D. S., Foulger, G. R., & Julian, B. R. (2009). The puzzle of the 1996 Bárðarbunga, Iceland earthquake: No volumetric component in the source mechanism. *Bulletin of the Seismological Society of America*, 99, 3077–3085.
- Tryggvason, K., Husebye, E. S., & Stefansson, R. (1983). Seismic image of the hypothesized Icelandic hotspot. *Tectonophysics*, 100, 97–118.
- Waldhauser, F. (2001). HypoDD: A program to compute double-difference hypocentre locations, U. S. Geological Survey, Open File Report 01-113.
- Waldhauser, F., & Ellsworth, W. L. (2000). A double-difference earthquake location algorithm: Method and application to the northern Hayward fault, California. *Bulletin of the Seismological Society of America*, 90(6), 1353–1368.
- Wolfe, C. J., Bjarnason, I. T., Vandecar, J., & Solomon, S. C. (1997). Seismic structure of the Iceland mantle plume. *Nature*, 385, 245–247.
- Zobin, V. M. (1999). The fault nature of the Ms 5.4 volcanic earthquake preceding the 1996 subglacial eruption of Grimsvötn volcano, Iceland. *Journal of Volcanology and Geothermal Research*, 92, 349–358.